Journal of Agricultural Engineering

https://www.agroengineering.org/

Air-suction double-roller harvesting device for *Lycium barbarum* L.

Yunlei Fan,[1,2] Zhuan Wu,[1] Naishuo Wei,[1] Ruiqi Yao,[1] Min Wang,[1] Jie Bai,[1] Wei Zhang,[1,2] Yanwu Jiang,[1] Zeyu Wang,[1] Yu Chen,[1] Jun Chen[1]

[1]College of Mechanical and Electronic Engineering, Northwest A&F University, Yangling, Shaanxi
[2]School of Mechanical Engineering, Qinghai University, Xining, China

Corresponding author: Jun Chen, College of Mechanical and Electronic Engineering, Northwest A&F University, Yangling, Shaanxi 712100, China. E-mail: chenjun_jdxy@nwsuaf.edu.cn

Please cite this article as doi: 10.4081/jae.2026.2038

Submitted: 13 November2025
Accepted: 14 July 2026

Air-suction double-roller harvesting device for *Lycium barbarum* L.

Yunlei Fan,[1,2] Zhuan Wu,[1] Naishuo Wei,[1] Ruiqi Yao,[1] Min Wang,[1]
Jie Bai,[1] Wei Zhang,[1,2] Yanwu Jiang,[1] Zeyu Wang,[1] Yu Chen,[1] Jun Chen[1]

[1]College of Mechanical and Electronic Engineering, Northwest A&F University, Yangling, Shaanxi
[2]School of Mechanical Engineering, Qinghai University, Xining, China

Corresponding author: Jun Chen, College of Mechanical and Electronic Engineering, Northwest A&F University, Yangling, Shaanxi 712100, China. E-mail: chenjun_jdxy@nwsuaf.edu.cn

Abstract

Lycium barbarum L. (*L. barbarum*) is a continuous-flowering and continuous-fruiting crop with thin and delicate fruit skin, necessitating multiple harvesting rounds. Currently, the harvesting of *L. barbarum* primarily relies on manual labor, leading to high labor demands and underscoring the urgent need for efficient, low-damage mechanized harvesting solutions. In this study, an air-suction double-roller harvesting device was designed. The harvesting mechanism operates by guiding *L. barbarum* into the picking zone *via* an airflow-induced suction stream, followed by gentle separation through a flexible double-roller structure. The fruit guiding process was modeled based on pneumatic attraction and analyzed through high-speed photography experiments. The results indicate that fruit velocity gradually increases during the guiding phase, with peak acceleration occurring at a specific location within this stage. A response-surface experiment was conducted to evaluate the effects of preloading force and roller speed on the picking rate of ripe fruit, the picking rate of unripe fruit, and the mechanical damage rate of ripe fruit. Parameter optimization resulted in optimal operating conditions with a preloading force of 0.903 N and a roller speed of 49.172 r/min. Under these conditions, validation experiments achieved a picking rate of ripe fruit of 93.7%, a picking rate of unripe fruit of 2.8%, and a damage rate of ripe fruit of 1.1%. This study provides a valuable reference for the design of vacuum-based harvesting devices for *L. barbarum*.

Key words: *lycium barbarum L.* harvesting; air-suction guidance; flexible double-roller mechanism; high-speed photography; response-surface experiment.

Introduction

The primary cultivation region for *L. barbarum* is located in northwestern China, where the fruit is rich in various nutritional components such as vitamins, polysaccharides, and carotenoids (Masci *et al.*, 2018; Patsilinakos *et al.*, 2018). *L. barbarum* is a continuous flowering and fruiting crop that requires multiple harvests during its production cycle. Currently, harvesting is primarily conducted through manual labor, which entails substantial workforce input and exhibits low efficiency. This operational limitation significantly hinders the development of the *L. barbarum* industry in China (Chen *et al.*, 2022; Chen *et al.*, 2024b; Jinpeng *et al.*, 2018; Ma *et al.*, 2020). The fruit of *L. barbarum* is highly susceptible to mechanical damage under significant compressive force, which compromises its market quality and reduces economic returns. Therefore, there is an urgent need to develop harvesting machinery that ensures high efficiency and minimal damage (Jiang *et al.*, 2025; Zhao *et al.*, 2019).

Scholars have conducted extensive exploratory research on the mechanized harvesting of goji berries, significantly promoting the advancement of mechanized harvesting technologies. Currently, the main harvesting mechanisms for *L. barbarum* are classified into three types: vibration-based, brush-vibration-based, and airflow-based systems (Chen *et al.*, 2019; Zhang *et al.*, 2018; Zhang *et al.*, 2015).In the research of *L. barbarum* vibration harvesters, Chen *et al*. (2024a) designed a vibration harvester and applied it in trellis cultivation plantations, achieving a mature fruit harvest rate of 86.44%. Qingyu *et al.* (2022) designed a vibration comb brush harvester, with a mature fruit harvest rate of 83.65%. Zhao *et al.* (2021) developed a vibration-brush type *L. barbarum* harvester, which integrates the principles of vibration and combing. Field trials demonstrated a ripe fruit harvesting rate of 85.8%. Wang *et al.* (2024) designed an interactive human-machine *L. barbarum* harvesting machine, which achieves high-efficiency picking through a multi-degree-of-freedom vibration picking arm. The integrated winnowing and collection functions enable a harvesting efficiency five times that of manual labor. Yu *et al*. (2024) investigated the optimal vibration frequency for *L. barbarum* harvesting, revealing that the harvesting efficiency peaks at 97.56% when the vibration frequency is maintained within the range of 8-14Hz. In the field of airflow harvesting machinery research, Chen *et al*. (2021) developed a pneumatic oscillation *L. barbarum* harvester. Experimental results indicate that at an outlet distance of 10 cm, an outlet airflow velocity of 70 m/s, and a vibration frequency of 2 Hz, the harvesting rate for mature fruits reached 85.21%. Wang *et al*. (2019) conducted experiments on the parameters of air suction picking of *L. barbarum*. Under the optimal working parameters, the time required for the *L. barbarum* to fall off was 1.92 s, which verified that the air suction method for picking *L. barbarum* is feasible. Harano *et al.* (2012) conducted a study on vacuum-assisted harvesting of blue honeysuckle berries, employing a rake mechanism for fruit detachment and utilizing negative pressure airflow for fruit collection. Lu *et al*. (2022) developed an apple-picking robot system based on the vacuum principle, which adopts a vacuum adsorption, twisting and pulling method to pick apples. Yang *et al.* (2022) has developed a vacuum negative pressure mushroom end-effector, achieving a harvesting success rate of 88.2% in factory environments. Wu *et al.* (2022) designed a tea oil flower harvesting device that combines the harvesting methods of friction roller torsion and pipeline air flow transportation. Hou *et al.* (2025) designed a pneumatic jujube picker. By the combined effect of the squeezing of the picking roller and the negative pressure airflow, the fruits can be picked. When the wind speed is 25 m/s and the rotational speed of the picking roller is 31 r/min, it can achieve efficient and low-loss harvesting of fresh jujubes.This paper designs a suction-driven dual-roller type *L. barbarum* picking device. The picking principle is to guide *L. barbarum* through suction and pick them with flexible double-roller. The *L. barbarum* guiding process is modeled and analyzed through high-speed photography experiments. Parameter experiments are carried out to clarify the main factors and rules affecting the picking effect. The optimal working parameter combination of the *L. barbarum* picking device is optimized and verified through validation experiments, which prove that the picking device can meet the agricultural requirements. This study provides a valuable reference for the design of vacuum-based harvesting devices for *L. barbarum*.

Materials and Methods

Overall structure and working principle

Overall structure

The air-suction double-roller *L. barbarum* harvesting device primarily comprises an air-suction plate, pulleys, a tension belt, a support frame, a driven roller, a driven gear shaft, a driving gear shaft, a protective casing, a driving roller, a DC reduction motor, a handle, and an outer housing. The overall structure is illustrated in Figure 1. The handle is connected to a *L. barbarum* collection container *via* a flexible hose, which in turn is linked to the fan's air inlet. The air-suction plate is positioned at the outermost end of the device and features a longitudinal slot aperture designed to guide the *L. barbarum* into the gap between the driving and driven rollers. The driving and driven rollers are mounted on the respective driving and driven gear shafts, which are fixedly supported by the support frame. Pulleys are freely fitted onto the gear shafts, with a tension belt installed between the pulleys on the driving and driven gear shafts. A corresponding elongated slot is incorporated into the support frame to accommodate movement. As the fruits enter the roller gap, the driven roller is displaced outward under pressure, causing the tension belt to elongate and consequently increasing the gap width accordingly. The protective casing prevents the rollers from entraining and damaging the harvested fruits. By integrating pneumatic suction guidance with a flexible dual-roller harvesting mechanism, the device significantly reduces the mechanical damage rate of fruits during the harvesting process.

Working principle and main technical parameters

During operation in the field, the picking device operates with the fan running continuously upon power activation. Airflow is drawn in through the elongated slot apertures of the air suction plate, directed through the handle into the collection chamber, and subsequently discharged via the fan outlet. The DC reduction motor drives the rotation of the driving gear shaft, which in turn rotates the driving roller. Power is transmitted from the driving gear shaft to the driven gear shaft through a meshing gear mechanism. Fruits are guided into the roller gap through the elongated slots of the air-suction plate. The self-adjusting pre-tensioned belt dynamically regulates the gap size according to the dimensions of individual *L. barbarum* fruits, enabling adaptive harvesting. Harvested fruits are conveyed to the collection box through a flexible conduit. The elastic compensation mechanism integrated within the pre-tensioned belt effectively mitigates mechanical damage resulting from variations in fruit size. Together with the directional airflow design of the air suction plate, this ensures orderly and controlled feeding of fruits into the roller assembly.Table 1 presents the main technical parameters of the air-suction double-roller *L. barbarum* harvesting device.

Design and parameter determination of key components

Modeling and analysis of the air-assisted guidance process

When the harvesting device approaches the fruit, the fruit undergoes deflection due to the aerodynamic drag force exerted by the airflow. As illustrated in Figure 2, under steady flow conditions, the fruit reaches a stable equilibrium state determined by three forces: its weight G, the airflow drag force F_D, and the tensile force F_L from the fruit stalk. The force balance condition in this state is given in Equation (1).

$$\begin{cases} F_D = G\dfrac{\sin^2 \alpha}{\cos \alpha} \\ F_L = G\tan \alpha \end{cases} \qquad \text{(Eq. 1)}$$

Where F_D denotes the drag force exerted on the fruit by the airflow. Under steady flow conditions, when the deflection angle satisfies $\alpha \in (0^\circ, 90^\circ)$, a larger swing angle α corresponds to a greater drag force F_D acting on the fruit. When the forces are in equilibrium, the method for calculating the airflow drag force is given in Equation (2).

$$F_D = \frac{1}{2} C_D A \rho v_r^2 \qquad \text{(Eq. 2)}$$

Where C_D denotes the drag coefficient, A represents the cross-sectional area of the fruit exposed to the airflow, ρ denotes the air density, and v_r denotes the relative velocity between the airflow and the fruit.

In the actual harvesting process, the suction-induced guidance of the fruit into the suction port is a dynamic process. The total kinetic energy acquired by the fruit from the moment it begins to experience the airflow drag force until it enters the suction port is given in Equation (3).

$$\int_0^L \left(\frac{1}{2}C_{Dx}A_x\rho v_{rx}^2 - G\frac{\sin^2 \alpha_x}{\cos \alpha_x}\right)dx = \frac{1}{2}mv_0^2 \qquad \text{(Eq. 3)}$$

Where L denotes the horizontal distance from the fruit to the suction port; C_{Dx}, A_x, and v_{rx} represent the drag coefficient, the cross-sectional area exposed to the airflow, and the horizontal relative velocity between the airflow and the fruit at the current position, respectively; α_x denotes the swing angle at that position, while v_0 represents the velocity of the fruit as it enters the suction port. Analysis indicates that an increase in fan flow rate results in a higher v_{rx}, which in turn leads to a greater entry velocity v_0 and increased kinetic energy prior to entering the suction port. The condition for successful airflow-guided transport of the fruit into the suction port is that $v_0>0$, and the fruit's velocity remains positive throughout the entire guidance process.

Air-suction plate

Based on agronomic parameter studies of *L. barbarum* cv. Ningqi No. 7, the average diameter of ripe fruits is 10.74 mm with a standard deviation of 1.81 mm, that of semi-ripe berries is 6.50 mm with a standard deviation of 1.00 mm, and that of green berries is 5.34 mm with a standard deviation of 0.98 mm. The dimensions of the elongated slot holes on the air-suction plate significantly influence fruit adsorption performance. When the length of the slots is fixed, an increased width facilitates easier entry of fruits into the gap between the rollers; however, it also requires a greater airflow volume from the fan. Similarly, longer slot lengths enable simultaneous harvesting of more fruits, thereby improving picking efficiency, but at the cost of higher airflow demand.

Considering the fan's negative pressure and airflow capacity, the edges of the slot holes are rounded to ensure stable adsorption of target fruits, minimize surface damage, and reduce fruit injury rates. The structural configuration of the elongated slot holes on the air-suction plate is illustrated in Figure 3. The optimized design parameters are as follows: slot width b = 14 mm, length l = 90 mm, and opening angle θ = 40°. The experimentally validated air-suction plate design enables effective airflow-guided transport and reliable adsorption of fruits into the roller gap.

Flexible double-roller assembly

After the *L. barbarum* are guided into the gap between the two rollers by the suction plate, the flexible rollers apply compressive force and friction to the fruits. When the frictional force exceeds the binding force of the fruit pedicel, the fruit detaches from the stalk and is conveyed through the pipeline to the collection box. As shown in Figure 4, upon entering the roller gap and neglecting the suction force, the forces acting on the fruit include the normal force F_n, the friction force F_f, and the tensile force F_T exerted by the fruit pedicel. F_0 denotes the preload force of the single-side pre-tensioned belt. When a single fruit enters the roller gap, the pressure applied to the *L. barbarum* is:

$$F_n = 2(F_0 + k\Delta L) \quad \text{(Eq. 4)}$$

Where *k* denotes the stiffness coefficient of the pre-tensioned belt, and ΔL represents the change in length of the pre-tensioned belt. Due to mechanical constraints, $\Delta L \leq 3\text{mm}$.

The condition for successful detachment of a single fruit during harvesting is:

$$F_T \leq F_{f\max} \quad \text{(Eq. 5)}$$

$$F_{f\max} = \mu F_n = 2\mu(F_0 + k\Delta L) \quad \text{(Eq. 6)}$$

$$F_T = F_J \quad \text{(Eq. 7)}$$

Among them, F_J represents the force required for fruit detachment from the pedicel. Substituting Eqs. (6) and (7) into Eq. (5):

$$2\mu(F_0 + k\Delta L) \geq F_J \quad \text{(Eq. 8)}$$

Suppose N fruits simultaneously enter the gap between the rollers and each fruit is subjected to the same pressure from the rollers; then the condition for successfully harvesting all N fruits is:

$$2\mu(F_0 + k\Delta L) \geq NF_J \quad \text{(Eq. 9)}$$

To avoid mechanical damage to the surface of the *L. barbarum* fruit, the roller is fabricated from food-grade silicone rubber with a Shore A hardness of 0° and a Young's modulus of 0.02 MPa, exhibiting excellent elasticity. The sliding friction coefficient μ between ripe *L. barbarum* fruits and silicone rubber was experimentally determined to be 2.15, with a standard deviation of 0.23. The average separation force F_J between mature goji berries and their pedicels is 0.84 N, with a standard deviation of 0.29 N.

High-speed photographic analysis of the gas-attracting guiding process

As shown in Figure 5a, a high-speed photographic test platform was established. To facilitate observation of the fruit guiding process, the *L. barbarum* harvesting device was fabricated using transparent resin material via 3D printing, and surrounding branches and leaves were removed to retain only a single fruit. The branch was fixed to align directly with the inlet of the harvesting device. The guiding process was recorded using a Qianyanlang X213 high-speed camera operating at 500 frames per second for a duration of 1 s. Key physical parameters of the tested *L. barbarum* specimen were as follows: fruit mass of 1.64 g, length of 24.07 mm, width of 12.38 mm, fruit stalk length of 25.68 mm, and distance from the geometric center of the fruit to the suction port of 17.90 mm. The static wind pressure at the handle of the harvesting device was -1.3 kPa. Upon activation of the negative pressure, the high-speed camera was simultaneously triggered to capture the guiding dynamics. The recorded video was analyzed using the Qianyanlang high-speed image analysis system, and the results are presented in Figure 5. Figure 5b depicts the initial moment when the fruit begins to swing, while Figure 5c illustrates the instant the fruit enters the suction port. Velocity and acceleration measurements during the air-attracting guiding phase were terminated upon fruit entry into the suction port. Figure 5d presents the velocity curve, showing a gradual increase in speed throughout the process, reaching 0.206 m/s at the point of entry. Figure 5e displays the acceleration curve, indicating significant variation during the process, with a peak acceleration of 2.751 m/s^2 occurring at an intermediate stage. The total air-attracting guiding time from the onset of fruit movement to complete entry into the suction port was 0.122 s, demonstrating that the pneumatic guidance process is highly efficient and requires minimal time.

Parameter experiment

Condition of experiment

To evaluate the operational performance of the air-suction double-roller *L. barbarum* harvesting device and identify the optimal parameter combination, a field experiment was conducted in July 2025 at the cultivation base of Zhengqihong *L. barbarum* Industry Development Co., Ltd. in Sanying Town, Yuanzhou District, Guyuan City, Ningxia Hui Autonomous Region (106°E, 36°N). The experimental cultivar was Ningqi No. 7, with trees aged 6 to 7 years. Planting row spacing was 2.8 m, plant spacing was 1.0 m, and average plant height was 1.6 m. On the day of the experiment, the fruit–pedicel separation force of *Lycium barbarum* L. cv. Ningqi No. 7 was measured.

Twenty ripe, semi-ripe, and green fruits were randomly sampled for each maturity stage. The mean fruit–pedicel separation force was 0.84±0.29 N for ripe fruits, 1.15±0.60 N for semi-ripe fruits, and 3.05±0.52 N for green fruits. Key experimental equipment included a prototype of the air-suction double-roller *L. barbarum* harvesting device, an intelligent digital micromanometer (Shanghai Yiou Instrument Equipment Co., Ltd., DP1000-IIIB; measurement range and accuracy specified), a vernier caliper (range: 200 mm), and a multifunctional electronic scale (accuracy: 0.001 g).

Experimental factors and evaluation indicators

The agronomic requirements for *L. barbarum* harvesting dictate that only fully ripe fruits should be collected, in order to prevent damage to ripe berries and minimize the harvest of unripe fruits. To maximize the harvesting rate of ripe fruits and optimize operational parameters for peak performance, a parameter optimization experiment was designed and conducted.

Before conducting the parameter optimization experiments, high-speed photography tests were performed to analyze the movement characteristics of wolfberry fruits under airflow guidance. The results showed that when the static wind pressure at the handle position of the harvesting device was set to −1.3 kPa, the airflow could effectively guide the fruits into the harvesting area and ensure stable fruit movement. Based on this working condition, preliminary experiments were conducted to evaluate the effects of different wind pressures on harvesting performance. The results indicated that, within the suitable working wind pressure range, variations in wind pressure had no significant effects on the mature fruit harvesting rate, immature fruit mis-harvesting rate, or mature fruit damage rate.

Therefore, to reduce the interaction among experimental factors and to focus on the effects of mechanical parameters on harvesting performance, the wind pressure was fixed at −1.3 kPa in the parameter optimization experiments. Consequently, the pretension force (X_1) of the tensioning belt and the rotational speed (X_2) of the counter roller were selected as the experimental factors. The harvesting rate of ripe fruits (Y_1), the mis-harvesting rate of unripe fruits (Y_2), and the damage rate of ripe fruits (Y_3) were selected as evaluation indicators, with their calculation methods detailed in Eqs. (10), (11), and (12). A two-factor, three-level experimental design was employed, with factor level coding presented in Table 2. The experimental layout and results are summarized in Table 3. A total of 12 experimental groups were performed, each repeated three times, and the average of the three replicates was used as the representative value for each group.

$$Y_1 = \frac{n_1}{n_1 + n_2} \times 100\% \qquad \text{(Eq. 10)}$$

$$Y_2 = \frac{n_3}{n_3 + n_4} \times 100\% \qquad \text{(Eq. 11)}$$

$$Y_3 = \frac{n_5}{n_1} \times 100\% \qquad \text{(Eq. 12)}$$

Among them, n_1 and n_2 denote the number of ripe fruits harvested and those not harvested, respectively; n_3 and n_4 denote the number of unripe fruits harvested and those not harvested, respectively; and n_5 denotes the number of damaged ripe fruits that were successfully harvested.

Results and Discussion

Parameter test results

Based on the experimental results presented in Table 3, a regression equation was developed using Design-Expert 12 software, with the harvesting rate of mature fruits as the response variable and the coded values of the factors as independent variables. The regression equation is as follows:

$$Y_1 = 93.5 + 2.79X_1 - 0.0492X_2 \quad \text{(Eq. 13)}$$

The analysis of variance (ANOVA) for the regression equation yields the results presented in Table 4. These results indicate that the model is statistically significant, with a *p*-value of 0.0001 ($p<0.05$). Among the factors, X_1 has a significant effect on the harvesting rate of mature fruits ($p<0.05$), whereas factor X_2 does not exhibit a significant influence. The *p*-value of the lack-of-fit test is greater than 0.05, indicating no significant lack of fit in the regression model.

Similarly, with the harvesting rate of unripe fruits as the response variable and the coded values of the factors as independent variables, the regression equation was derived, and its expression is as follows:

$$Y_2 = 3.14 + 4.08X_1 + 0.9026X_2 + 0.6315X_1X_2 + 0.9799X_1^2 + 1.11X_2^2 \quad \text{(Eq. 14)}$$

The analysis of variance (ANOVA) for the regression equation yields the results presented in Table 5. These results indicate that the model is statistically significant, with a *p*-value less than 0.0001 ($p<0.05$). Among the factors, X_1, X_2, X_1^2, and X_2^2 have a significant effect on the mis-harvesting rate of unripe fruits ($p<0.05$), whereas the interaction term X_1X_2 does not exhibit a significant influence. The p-value of the lack-of-fit test is greater than 0.05, indicating no significant lack of fit in the regression model.

Similarly, with the damage rate of mature fruits as the response variable and the coded values of the factors as independent variables, the regression equation was derived, and its expression is as follows:

$$Y_3 = 1.15 + 2.68X_1 + 0.3699X_2 + 0.2507X_1X_2 + 1.91X_1^2 + 0.2456X_2^2 \quad \text{(Eq. 15)}$$

The analysis of variance (ANOVA) for the regression equation yields the results presented in Table 6. These results indicate that the model is statistically significant, with a *p*-value less than 0.0001 ($p<0.05$). Among the factors, X_1, X_2, and X_1^2 have a significant effect on the damage rate of mature fruits ($p<0.05$), whereas the other terms do not exhibit significant influence. The p-value of the lack-of-fit test is greater than 0.05, indicating no significant lack of fit in the regression model.

By analyzing the influence of various factors on the harvesting rate of mature fruits, the response surface is shown in Figure 7a. According to Eq. (13) and Table 4, the pretensioning force has the greatest effect on the harvesting rate of mature fruits, whereas the rotational speed exhibits no significant influence. As illustrated in Figure 7a, the harvesting rate increases with increasing pretensioning force. This is because a higher pretensioning force enhances the frictional force exerted by the flexible rollers on the fruits, thereby improving picking success. By analyzing the influence of various factors on the mis-harvesting rate of unripe fruits, the corresponding response surface is presented in Figure 7b. Based on Eq. (14) and Table 5, the pretensioning force exerts the most significant effect on the mis-harvesting rate, while the rotational speed has a relatively minor impact. No significant interaction effect exists between the pretensioning force and rotational speed. As shown in Figure 7b, the mis-harvesting rate increases with increasing pretensioning force. This occurs because greater pretensioning force leads to higher friction, making unripe fruits more likely to be harvested unintentionally. Additionally, as rotational speed increases, the mis-harvesting rate rises slightly due to enhanced dynamic interaction.By analyzing the influence of various factors on the damage rate of mature fruits, the response surface is displayed in Figure 7c. From Eq. (15) and Table 6, it is evident that the pretensioning force has the strongest effect on fruit damage, followed by rotational speed. There is no significant interaction among the factors. As depicted in Figure 7c, the damage rate increases with increasing pretensioning force. This is attributed to higher compressive pressure on the fruits, which raises the likelihood of mechanical compression damage. Furthermore, as rotational speed increases, the damage rate also increases slightly. This is because higher rotational speed increases the probability of slippage between the *L. barbarum* and the flexible rollers. When slippage occurs, the berry surfaces are more prone to scratching, leading to an elevated damage rate.

Parameter optimization and experimental verification

To optimize the parameters of the harvesting device and validate them experimentally, Design-Expert 12 software was employed to simultaneously optimize three evaluation criteria: the harvesting rate of mature fruits (Y_1), the mis-harvesting rate of unripe fruits (Y_2), and the damage rate of mature fruits (Y_3). The objective function, defined in Eq. (16), reflects the primary goal of the air-suction double-roller harvesting mechanism -maximizing the harvesting rate of mature fruits. Accordingly, the weight distribution ratio of the three indicators was empirically set at 4:3:3.

$$Y = \begin{cases} \max Y_1(X_1, X_2) \\ \min Y_2(X_1, X_2) \\ \min Y_3(X_1, X_2) \\ 0.9N \leq X_1 \leq 1.2N \\ 40\,\mathrm{r\,min^{-1}} \leq X_2 \leq 80\,\mathrm{r\,min^{-1}} \end{cases} \quad \text{(Eq. 16)}$$

The optimal combination of parameters was obtained by solving Eq. (16), yielding a preload force of 0.903 N and a rotational speed of 49.172 r/min. To validate the optimized parameters, a verification experiment was conducted using rounded values - 0.9 N for preload force and 50 r/min for rotational speed. The experiment was performed on July 20, 2025. To minimize random experimental errors, each test was repeated five times. The verification results showed that the harvesting rate of mature fruits reached 93.7%, the mis-harvesting rate of unripe fruits was 2.8%, and the damage rate of mature fruits was 1.1%.

Conclusions

Based on the principle of air-suction fruit guidance and flexible double-roller harvesting, this study presents an air-suction double-roller *L. barbarum* harvesting device. Theoretical analysis indicates that for *L. barbarum* to be successfully guided into the suction port, their velocity during the guiding process must remain greater than zero. High-speed photography experiments reveal that the berry velocity increases throughout the process, with maximum acceleration occurring at a specific moment.

The response surface methodology was employed to design experiments involving two key parameters -preload force and roller speed- to evaluate their effects on the harvesting rate of mature fruits, the mis-harvesting rate of unripe fruits, and the damage rate of mature goji berries. Following optimization, the optimal parameter combination was determined to be a preload force of 0.903 N and a roller speed of 49.172 r/min. Verification experiments demonstrated that under these conditions, the harvesting rate of ripe fruit reached 93.7%, the mis-harvesting rate of unripe fruit was 2.8%, and the damage rate of ripe fruit was 1.1%, meeting the requirements for low-damage harvesting. This research provides a reference for the design of air-suction *L. barbarum* harvesting devices.

Competing interest

The authors declare no conflict of interest.

Authors' contributions

Yunlei Fan, conceptualization, data curation, methodology, validation, writing – original draft, writing – review and editing. **Naishuo Wei,** investigation, visualization, writing – review and editing. **Zhuan Wu**, investigation, visualization, writing – review and editing. **Ruiqi Yao,** conceptualization, software. **Jie Bai,** formal analysis. **Zeyu Wang,** formal analysis. **Min Wang**, writing – review and editing. **Yanwu Jiang,** investigation. **Jun Chen,** methodology, funding acquisition, writing – original draft, writing – review and editing. **Yu Chen,** methodology, funding acquisition, writing – original draft, writing – review and editing. **Wei Zhang,** supervision.

All authors read and approved the final version of the manuscript and agreed to be accountable for all aspects of the work.

Funding

This study was supported by the National Natural Science Foundation of China (32272001) and Key Research and Development and Transformation Program of Qinghai Province (2024-NK-141S-1).

Data Availability Statement

The data used to support the findings of this study are available from the corresponding author on reasonable request.

References

Chen J, Zhao J, Chen Y, Bu LX, Hu GR, Zhang EY, 2019. Design and experimental optimization of vibrating-brush type wolfberry harvester. Trans Chin Soc Agric Mach 50:11.

Chen QY, Kang R, Wei NS, Fan YL, Wang ZY, Chen Y, Chen J, 2024a. Design and experiment optimize of the vibration harvesting machine of Lycium barbarum L. J Agric Eng 55:1597.

Chen QY, Zhang SX, Hu GR, Zhou JG, Zhao J, Chen Y, et al., 2022. Parameter optimization of the harvest method in the standardized hedge cultivation mode of Lycium barbarum using response surface methodology. Horticulturae 8:308.

Chen QY, Zhang SX, Wei NS, Li PH, Hu GR, Chen J, Chen Y, 2024b. Design and optimization of torsion harvester of Lycium barbarum L. Int J Agric Biol Eng 17:109-115.

Chen Y, Zhao J, Hu G, Chen J,2021. Design and testing of a pneumatic oscillating chinese wolfberry harvester. Horticulturae 7:214.

Harano Y, Ozima M, Araya K, Teramoto C, Wakita Y, Nishino T, et al., 2012. Haskaop harvester: part 3: prototypical model. Appl Eng Agric 5:15-19.

Hou HM, Niu W, Wen QX, Yang HR, Zhang JM, Zhang R, et al., 2025. Design and testing of a pneumatic jujube harvester. Agronomy 15:1881.

Jiang YW, Chen QY, Wei NS, 2025. Determining the impact bruising of goji berry using a pendulum method. Horticulturae 11:14.

Jinpeng W, Song M, Hongru X, Ying Z, Hongping Z, 2018. Research on mechanized harvesting methods of Lycium barbarum fruit. IFAC-PapersOnLine 51:223-226.

Lu R, Dickinson N, Lammers K, Zhang K, Chu P, Li Z, 2022. Design and evaluation of end effectors for a vacuum-based robotic apple harvester. J ASABE 65:963-974.

Ma F, Li L, Wang Y, Li P, Zhu C, 2020. Biomechanical properties of wolfberry plant organs. Eng Agric 40:162-176.

Masci A, Carradori S, Casadei MA, Paolicelli P, Petralito S, Ragno R, Cesa S, 2018. Lycium barbarum polysaccharides: Extraction, purification, structural characterisation and evidence about hypoglycaemic and hypolipidaemic effects. A review. Food Chem 254:377-389.

Patsilinakos A, Ragno R, Carradori S, Petralito S, Cesa S, 2018. Carotenoid content of Goji berries: CIELAB, HPLC-DAD analyses and quantitative correlation. Food Chem 268:49-56.

Qingyu C, Shixia Z, Guangrui H, Jianguo Z, Jian Z, Yu C, et al., 2022. Parameter optimization of the harvest method in the standardized hedge cultivation mode of Lycium barbarum using response surface methodology. Horticulturae 8:308.

Wang RY, Zheng ZA, Xu LM, Wu G, Chen JW, Yuan QC, et al., 2019. Experimental study on parameters of pneumatic suction harvesting for Lycium barbarum. J Agric Mech Res 41:165-171.

Wang YT, Yang C, Gao YY, Lei YQ, Ma LF, Qu AL, 2024. Design and Testing of an Integrated Lycium barbarum L. harvester. Agriculture 14:1370.

Wu Z, Li L, Zhao Q, Guo X, Li JJA, 2022. Design and research of a harvesting actuator for Camellia oleifera flowers during the budding period. 12:1698.

Yang S, Ji J, Cai H, Chen H, 2022. Modeling and force analysis of a harvesting robot for button mushrooms. IEEE Access 10:78519-78526.

Yu ZH, Wu J, Jiang F, Xing H, Yan L, Yang JH, 2024. Kinematic analysis of the vibration harvesting process of Lycium barbarum L. fruit. Agriculture 14:1715.

Zhao J, Ma T, Inagaki T, Chen Y, Hu GR, Wang ZW, et al., 2021. Parameter optimization of vibrating and comb-brushing harvesting of Lycium barbarum L. based on FEM and RSM. Horticulturae 7 286.

Zhao J, Sugirbay A, Chen Y, Zhang S, Liu FY, Bu LX, et al., 2019. FEM explicit dynamics simulation and NIR hyperspectral reflectance imaging for determination of impact bruises of Lycium barbarum L. Postharvest Biol Technol 155:102-110.

Zhang WQ, Li ZZ, Tan YZ, Li W, 2018. Optimal design and experiment of variable-spacing comb-brush type wolfberry harvesting device. Trans Chin Soc Agric Mach 49:83-90.

Zhang Z, Xiao HR, Ding WQ, Mei S, 2015. Simulation analysis of vibration picking mechanism for Lycium barbarum and prototype test. Trans Chin Soc Agric Eng 31:20-28.

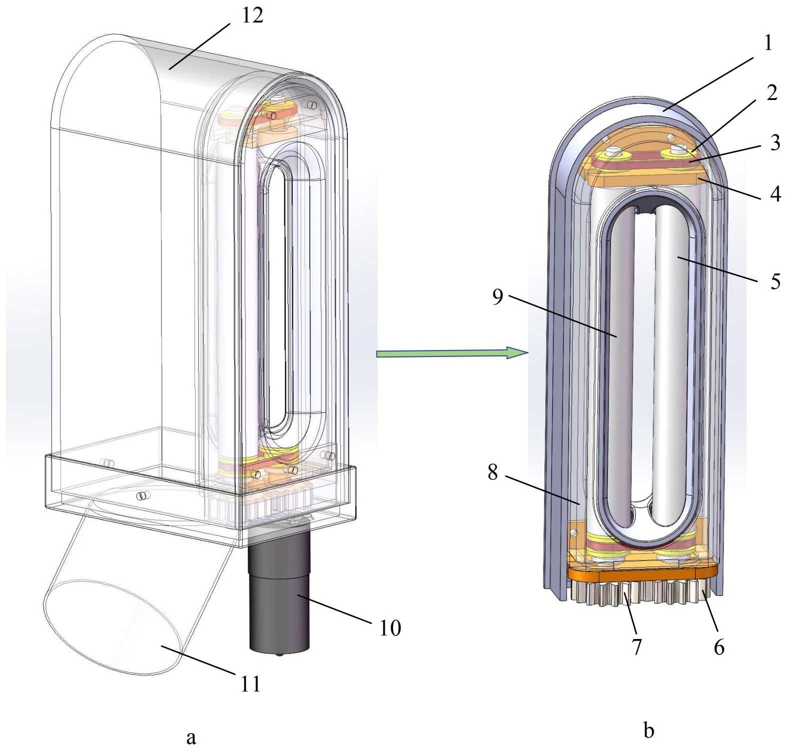

Figure 1. Schematic diagram of the air-suction double-roller harvesting device. Whole (**a**) and part (**b**) view. 1. Air-suction plate; 2. pulley; 3. tension belt; 4. support frame; 5. driven roller; 6. driven gear shaft; 7. driving gear shaft; 8. protective casing; 9. driving roller; 10. DC reduction motor; 11. handle; 12. outer housing.

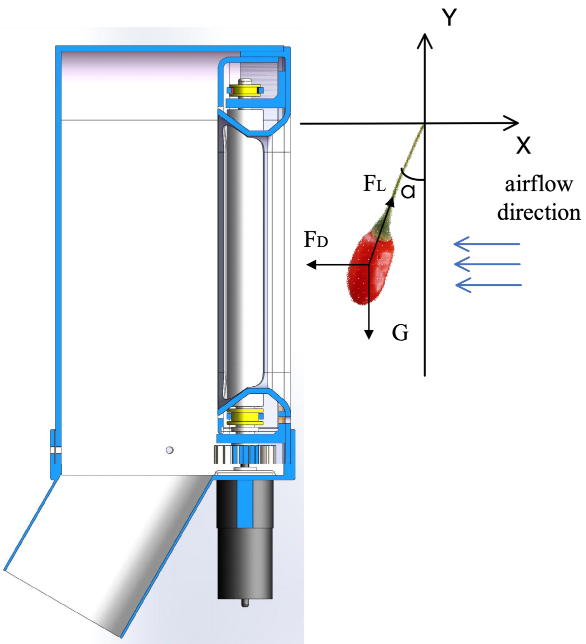

Figure 2. Schematic diagram of force analysis of air guide *L. barbarum.*

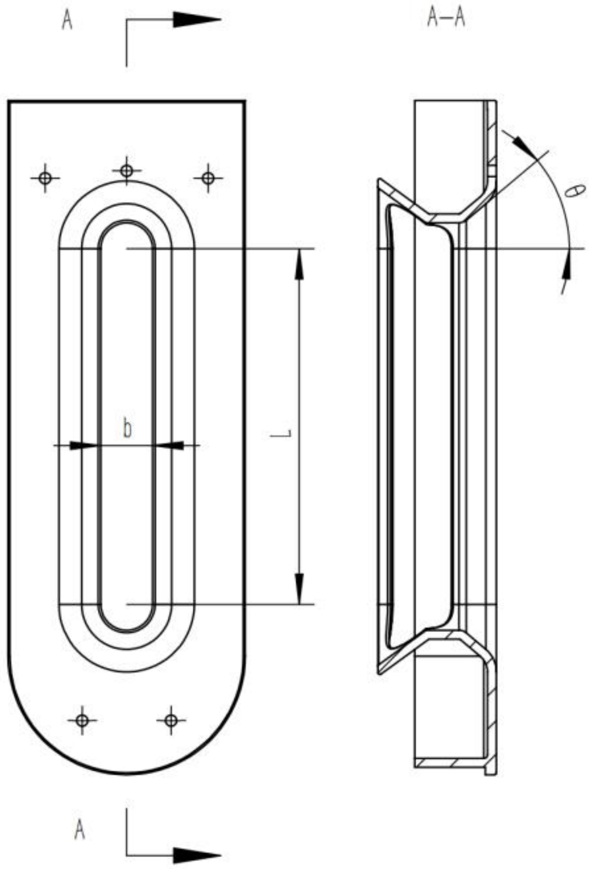

Figure 3. Schematic diagram of the air-suction plate structure.

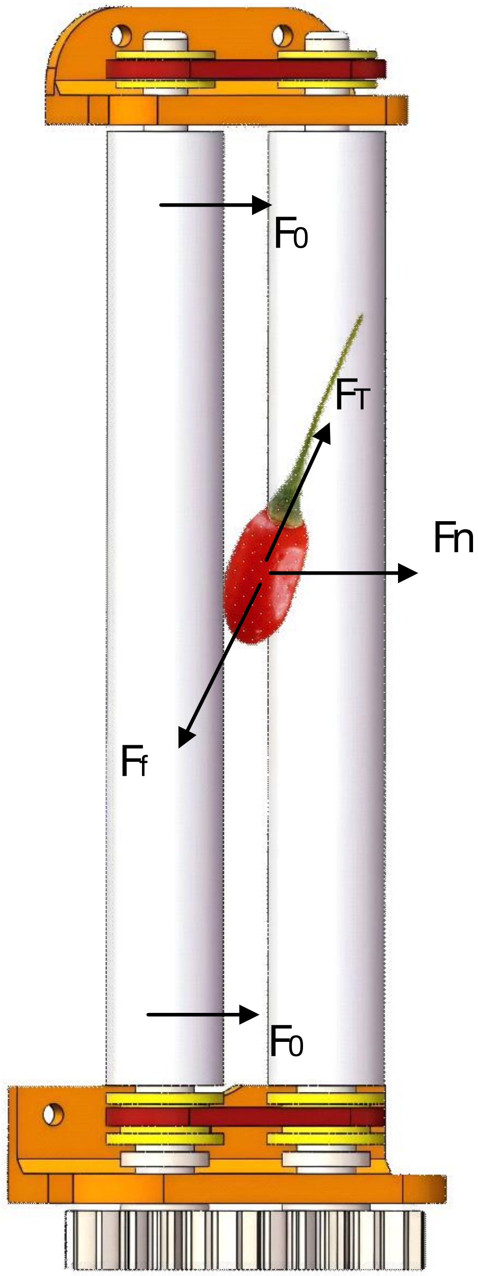

Figure 4. Schematic diagram of flexible double-roller picking fruit.

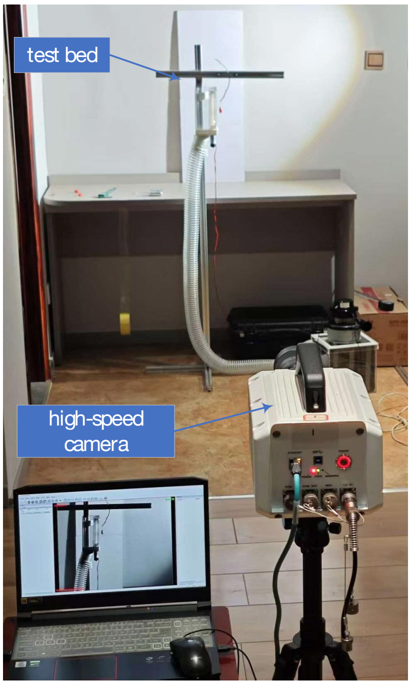

a

Velocity/ms^{-1}

Frame number

d

b

Accelerated velocity/ms^{-2}

Frame number

e

c

Figure 5. High-speed photographic analysis of the air-attracting guiding process: (**a**) experimental site, (**b**) initial moment, (**c**) final moment, (**d**) velocity curve, and (**e**) acceleration curve.

Figure 6. Field experiment.

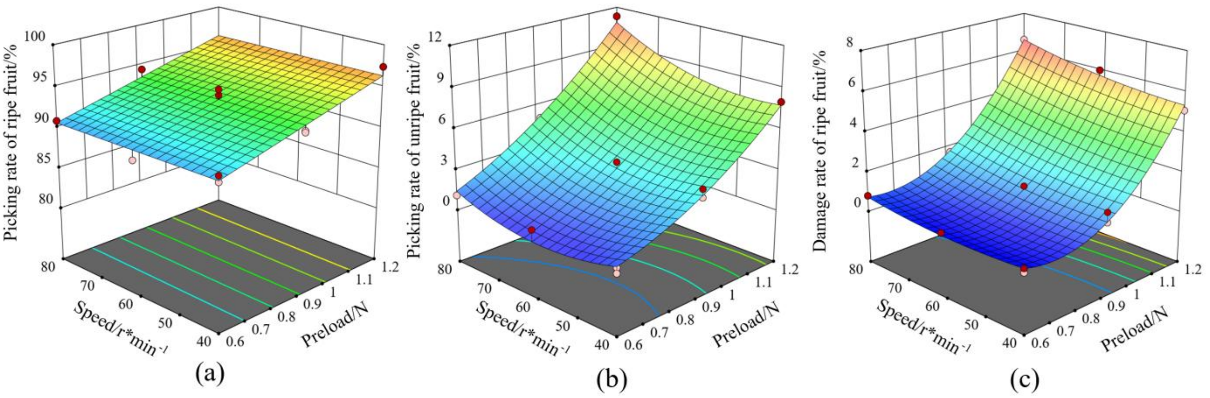

Figure 7. Response surface plots: (**a**) Influence of interaction factors on the picking rate of ripe fruits. (**b**) Influence of interaction factors on the picking rate of unripe fruits. (**c**) Influence of interaction factors on the Damage rate of unripe fruits.

Table 1. Main technical parameters of the harvesting device.

Parameters	Value
Fan power/w	1200
Maximum airflow rate of the fan(L/min)	3500
Maximum negative pressure of the fan/Kpa	28
Dimensions of the collection box （mm×mm×mm）	250×250×250
Inner diameter and length of the hose （mm×mm）	60×1500
Variable range of roll gap/mm	8-11
Roll diameter/mm	16
Width of the slot aperture on the air suction plate/mm	14
Maximum speed of DC gear motor (r/min)	120

Table 2. The codes of factors.

Codes	Preload X_1 （N）	Speed X_2 （r/min）
-1	0.6	40
0	0.9	60
1	1.2	80

Table 3. The experiment schemes and results.

Number	X_1 (N)	X_2 (r/min)	Y_1 (%)	Y_2 (%)	Y_3 (%)
1	1	0	95.9	7.5	6.0
2	0	1	94.4	5.0	1.7
3	0	-1	92.7	3.8	1.0
4	-1	1	90.9	1.1	0.8
5	-1	-1	91.3	0.8	0.3
6	0	0	94.7	2.5	1.3
7	0	-1	92.9	3.2	1.5
8	-1	0	89.5	0.9	0.5
9	-1	-1	90.6	0.4	0.5
10	1	1	95.0	11.3	6.6
11	1	-1	97.4	8.0	5.1
12	0	0	94.0	3.6	0.6

Table 4. ANOVA of the picking rate of ripe fruit.

Sources	Sum of squares	Degree of freedom	Mean square	F	*p*
Model	53.73	2	26.87	28.82	0.0001
X_1	53.24	1	53.24	57.11	<0.0001
X_2	0.0183	1	0.0183	0.0197	0.8916
Lack of fit	7.88	6	1.31	7.73	0.0609
Pure error	0.5100	3	0.1700		
Total	62.12	11			

Table 5. ANOVA of the picking rate of unripe fruit.

Sources	Sum of squares	Degree of freedom	Mean square	F	*p*
Model	124.15	5	24.83	55.24	<0.0001
X_1	110.27	1	110.27	245.31	<0.0001
X_2	5.94	1	5.94	13.21	0.0109
X_1X_2	1.86	1	1.86	4.14	0.0882
X_1^2	2.70	1	2.70	6.02	0.0496
X_2^2	3.14	1	3.14	6.99	0.0384
Lack of fit	1.83	3	0.6107	2.12	0.2767
Pure error	0.8650	3	0.2883		
Total	126.85	11			

Table 6. ANOVA of the damage rate of to ripe fruit.

Sources	Sum of squares	Degree of freedom	Mean square	F	*p*
Model	58.34	5	11.67	93.04	<0.0001
X_1	47.70	1	47.70	380.39	<0.0001
X_2	0.9972	1	0.9972	7.95	0.0304
X_1X_2	0.2931	1	0.2931	2.34	0.1772
X_1^2	10.24	1	10.24	81.67	0.0001
X_2^2	0.1541	1	0.1541	1.23	0.3101
Lack of fit	0.3624	3	0.1208	0.9293	0.5233
Pure error	0.3900	3	0.1300		
Total	59.09	11			